https://doi.org/10.5194/egusphere-2025-1793
Preprint. Discussion started: 6 May 2025

The role of the tropical carbon balance in determining the large atmospheric CO_2 growth rate in 2023

Liang Feng[1,2], Paul I. Palmer[1,2], Luke Smallman[1,2], Jingfeng Xiao[3], Paolo Cristofanelli[4], Ove Hermansen[5], John Lee[6], Casper Labuschagne[7], Simonetta Montaguti[4], Steffen M. Noe[8], Stephen M. Platt[5], Xinrong Ren[9], Martin Steinbacher[10], Irène Xueref-Remy[11]

1: University of Edinburgh, Edinburgh, EH9 3FF, UK.
2: National Centre for Earth Observation, University of Edinburgh, Edinburgh, EH9 3FF, UK.
3: Earth Systems Research Center, University of New Hampshire, Durham, NH 03824, USA.
4: National Research Council of Italy - Institute for Atmospheric Sciences and Climate, I-40129 Bologna, Italy.
5: Norwegian Institute for Air Research, Instituttveien 18, 2007 Kjeller, Norway.
6: School of Forestry, CRSF, University of Maine, ME, 04469, USA.
7: South African Weather Service, Cape Point research station, Stellenbosch 7599, South Africa.
8: Institute of Forestry and Engineering, Estonian University of Life Sciences, 51014 Tartu, Estonia.
9: NOAA Air Resources Laboratory Atmospheric Sciences and Modeling Division, College Park, MD 20740, USA.
10: Laboratory for Air Pollution / Environmental Technology, Swiss Federal Laboratories for Materials Science and Technology (Empa), 8600 Duebendorf, Switzerland.
11: Institut Méditerranéen de Biodiversité et d'Ecologie marine et continentale, Aix-Marseille Univ, Avignon Univ, CNRS, IRD, 13397 Marseille, France.

Correspondence to: Liang Feng (liang.feng@ed.ac.uk) and Paul Palmer (pip@ed.ac.uk)

Abstract. The global annual mean atmospheric CO_2 growth rate in 2023 was one of the highest since records began in 1958, comparable to values recorded during previous major El Niño events. We do not fully understand this anomalous growth rate, although a recent study highlighted a role for boreal North American forest fires. We use a Bayesian inverse method to interpret global-scale atmospheric CO_2 data from the NASA Orbiting Carbon Observatory. The resulting *a posteriori* CO_2 flux estimates reveal that from 2022 to 2023 the biggest changes in CO_2 fluxes of net biosphere exchange (NBE) – for which positive values denote a flux to the atmosphere – were over the land tropics. We find that the largest NBE increase is over eastern Brazil, with small increases over southern Africa and Southeast Asia. We also find significant increases over southeast Australia, Alaska, and western Russia. A large NBE increase over boreal North America, due to fires, is driven by our *a priori* inventory, informed by independent data. The largest NBE reductions are over western Europe, USA, and central Canada. Our NBE estimates are consistent with gross primary production estimates inferred from satellite observations of solar induced fluorescence and with satellite observations of vegetation greenness. We find that warmer temperatures in 2023 explain most of the NBE change over eastern Brazil, with hydrological changes more important elsewhere across the tropics. Our results suggest that ongoing environmental degradation of the Amazon is now playing a substantial role in increasing the global atmospheric CO_2 growth rate.

https://doi.org/10.5194/egusphere-2025-1793
Preprint. Discussion started: 6 May 2025

1 Introduction

The annual mean growth rate of atmospheric carbon dioxide (CO_2) is widely used as a zeroth order metric to determine the health of our planet. Even from the first few years' worth of data collected at Mauna Loa in the late 1950s it was plain to see that a) land vegetation imposed a large seasonal cycle on atmospheric CO_2 via photosynthesis and respiration, and b) combustion of fossil fuels led to a planetary scale impact on the atmosphere (Keeling, 1960; Keeling et al., 1976). Changes in the annual accumulation of atmospheric CO_2 (growth rate), the magnitude and phase of the seasonal cycle, and how they vary geographically, provide important clues about economic activity and the health of the land biosphere (Keeling et al., 1996; Graven et al., 2013; Barlow et al., 2015). These changes are inextricably linked, e.g., elevated uptake by the land biosphere will influence the annual growth rate as well as the seasonal cycle (e.g., Ainsworth and Rogers, 2007). On a global scale, using mass balance arguments, we know that only about 44% of fossil fuel emissions of CO_2 remain in the atmosphere (the airborne fraction) (Bennett et al., 2024) with the land biosphere and oceans absorbing the other 56%, approximately equally but with substantial year to year changes (Friedlingstein et al., 2023). The quasi-stability of the airborne fraction suggests that the land biosphere and the oceans absorb a progressively larger absolute amount of CO_2 from the atmosphere. We have an incomplete understanding of where this carbon is being absorbed and the stability of the resulting accumulated terrestrial carbon reservoirs against future changes in climate, e.g. Armstrong McKay et al., (2022). Consequently, years in which there are anomalously large annual mean CO_2 growth rates prompt concern from the scientific community. This concern grows when state-of-the-art process-based land biosphere models cannot forecast or explain these anomalies (Kondo et al., 2020).

Figure 1 shows the annual mean CO_2 growth rates reported by NOAA on a global scale, determined by combining data collected at sites across the globe, and from Mauna Loa in Hawaii (19.5ºN, 155.6ºW), USA, a site typically assumed to be representative of changes in the northern hemisphere carbon cycle (Buermann et al., 2007). The global picture shows that 2023 (Figure 1a) had one of the largest CO_2 growth rates on record, typically associated with the El Niño phase of ENSO, e.g., 1986, 1997/1998, and 2015/2016. What is also evident is a progressive increase in the annual growth rates from the 1950s (Figure 1c). Even anomalous values recorded in the last quarter of the 20th century are close to the median value from the 21st century (Figure 1c). The corresponding data collected at Mauna Loa shows a slightly different picture for the annual CO_2 growth rate (Figure 1b). At this site, the growth rate in 2023 was the largest on record, exceeding the past peak growth during 1997/1998 El Niño, attributed to extensive burning of peat over Southeast Asia (Page et al., 2002), and the 2015/2016 El Niño (Liu et al., 2017). At Mauna Loa, progressive changes in the growth rates are slightly more exaggerated than global mean values (Figure 1b,d), suggesting a larger role for tropical latitudes.

Data-driven top-down flux inversions allow us to attribute these observed changes in the atmospheric CO_2 growth rate to regional changes in surface carbon fluxes. Estimating regional carbon fluxes from atmospheric data requires an atmospheric

https://doi.org/10.5194/egusphere-2025-1793
Preprint. Discussion started: 6 May 2025

transport model that describes the physical relationship between surface CO_2 fluxes and the resulting atmospheric distribution of CO_2, *a priori* estimates of the distribution and magnitude of fluxes, and a Bayesian inference method that fits this model to the data accounting for model and data uncertainties (Tans et al., 1990; Baker et al., 2006; Gurney et al., 2002, 2004). Using an atmospheric transport model introduces additional errors (Schuh et al., 2019; Oda et al., 2023) but it remains an essential tool for interpreting the atmospheric data. Satellite observations of atmospheric CO_2 have challenged current understanding of the carbon cycle (Liu et al., 2017; Chatterjee et al., 2017; Patra et al., 2017; Palmer et al., 2019; Wang et al., 2020; Basso et al., 2023; Hugelius et al., 2024; O'Sullivan et al., 2024; Liu et al., 2024). They have primarily achieved this by collecting data over geographical regions that are not well covered by ground-based networks, particularly over the land tropics. These datasets are typically available with a time lag of only a few months, enabling us to explain the reasons behind anomalous annual CO_2 growth rates within a year of them happening.

To interpret recent annual changes in the CO_2 growth rate, we use the global 3-D GEOS-Chem atmospheric transport model and an ensemble Kalman filter to adjust our *a priori* distribution of CO_2 flux estimates to fit *in situ* and satellite observations of atmospheric CO_2. These methods and data are described in the next section. We report our results in section 3 and conclude our study in section 4.

2 Data and Methods

Here, we describe the modelling framework we use to infer *a posteriori* spatial distributions of CO_2 fluxes from atmospheric data and *a priori* inventories flux estimates, the atmospheric data, and the auxiliary atmospheric and land surface we use to evaluate the *a posteriori* flux estimates.

2.1 Inversion Framework

We use the GEOS-Chem global 3-D chemistry transport model of version 13.4 to provide the relationship between the surface fluxes and changes in atmospheric CO_2. For the experiments we report, we run the model at a horizontal resolution of 2° (latitude) × 2.5° (longitude), driven by MERRA2 meteorological reanalyses from the Global Modeling and Assimilation Office (GMA) based at NASA Goddard Space Flight Center (GSFC).

We use *a priori* CO_2 flux inventories, which include year-specific monthly biomass burning emission (GFEDv4.1; Randerson et al., 2017), and year-specific monthly anthropogenic emissions (ODIAC; Oda et al., 2018; Oda and Maksyutov, 2021). The anthropogenic emission estimates were extended to 2023 under the assumption that these emissions from the southern hemisphere remain stable between 2022 and 2023 but increased by 1.4% over the northern hemisphere based on data reported in the 2024 Statistical Review of World Energy by the Energy Institute. We use year-specific

https://doi.org/10.5194/egusphere-2025-1793
Preprint. Discussion started: 6 May 2025

terrestrial biosphere fluxes with a temporal resolution of three hours (CASA; Olsen and Randerson, 2004) up to the end of 2018, and repeat values for 2018 in subsequent years. We use monthly climatological ocean fluxes (Takahashi et al., 2009).

We use an established EnKF framework (Feng et al., 2009, 2017; Palmer et al., 2019) to estimate surface CO_2 fluxes from atmospheric CO_2 data collected by a satellite and a global *in situ* ground-based observation network, 2014—2023, inclusively. We define our land sub-regions by further dividing each of the 11 TransCom-3 land regions (Gurney et al., 2002) into 30 nearly equal sub-regions, with the exception for temperate Eurasia that has been divided into 56 sub-regions, due to its large landmass. We divide the 11 TransCom-3 ocean regions into 132 sub-regions. Our state vector includes monthly scaling factors for 488 regional pulse-like basis functions that describe natural CO_2 fluxes, including 356 land regions and 132 oceanic regions (Figure A1). The inversion framework and the experiments we report here closely follow our previous work (Palmer et al., 2019; Feng et al., 2022; Oda et al., 2023; Feng et al., 2023), and we assimilate *in situ* data and column averaged CO_2 dry-air mole fraction (X_{CO2}) retrievals from the NASA Orbiting Carbon Observatory (OCO-2), as described below.

2.2 In situ and OCO-2 atmospheric CO_2 data

We use version v11r of OCO-2 retrievals of column average dry air mole fraction (XCO2) from the JPL-ACOS team (Taylor et al., 2023). We only assimilate the nadir and glint observations over land, considering possible bias between the land and ocean XCO2 data. The consequent poor observational coverage over the ocean could result in the disaggregation of the land and ocean CO_2 fluxes being more sensitive to the *a priori* ocean flux inventory. Through sensitivity studies we find that our land CO_2 flux anomalies are not significantly sensitive to the to the *a priori* ocean flux inventory (not shown) or to the absence of OCO-2 glint data (Figure A2). To reduce the computational costs and error correlations, we thinned the OCO-2 observations to ensure a minimal time interval of 10 s.

We also assimilate *in situ* measurements of CO_2 mole fraction data from a subset of 113 sites (Figure A1) included in the NOAA GLOBALVIEWPlus 8.0 data product (Schuldt et al., 2022), incorporating data from the Integrated Carbon Observation System (ICOS RI et al., 2024).

2.3 GOSIF Gross Primary Productivity

We use a global gross primary production (GPP) product that is based on OCO-2 solar induced fluorescence (GOSIF) and linear relationships between SIF and GPP (Li and Xiao, 2019). We chose this data product, available globally a spatial resolution of 0.05° and a temporal resolution of eight days, because it is close to the median of observation-derived GPP estimates (Li and Xiao, 2019) and is available over our study period. The mean annual global total (2000-2023) is 135.5 ± 8.8 Pg C yr^{-1}, with a significant upward trend over the northern hemisphere. Comparisons show that this GPP data product is highly correlated (R^2=0.74) with GPP measurements collected at 91 eddy covariance flux sites across the globe. Here, we

https://doi.org/10.5194/egusphere-2025-1793
Preprint. Discussion started: 6 May 2025

use the monthly mean dataset and re-grid it to a regular one-degree grid to compare it with other variables including our *a posteriori* CO_2 flux estimates.

2.4 Gravity Recovery And Climate Experiment data

The GRACE space mission was jointly developed by NASA and DLR (German Space Agency) and launched into space in 2002. It measures temporal variations of the Earth's gravity field by tracking, using a K-band ranging system, the inter-satellite range and range rate between two coplanar, low altitude satellites (Tapley et al., 2004). The GRACE Science Data System uses these measurements, along with ancillary data, to estimate monthly (or sub-monthly) time series of global Earth's gravity fields (Bettadpur, 2007; Flechtner, 2007). Here, we use the NASA GRCTellus GRACE land product (RL06.2) for monthly total water storage (liquid water equivalent depth) at 1° × 1° global grids from January 2014 through March 2024 (http://grace.jpl.nasa.gov/). We have used these data in our previous studies, e.g., Feng et al., (2022, 2023).

2.5 NASA Meteorological Reanalyses

We use surface temperature (TS), specific humidity (SH), soil moisture in the top 0—10 cm (ground wetness, WET) datasets from MERRA2 developed by the GMAO at NASA GSFC to study environmental changes from 2010 to 2023. We calculate the vapour pressure deficit (VPD) from the 10-m MERRA2 temperature, and specific humidity following Fang et al., (2022). We have used these reanalyses data previously to study *a posteriori* CO_2 fluxes (Palmer et al., 2019) and methane emissions (Feng et al., 2022, 2023).

3 Results

Figure 2 shows *a posteriori* net fluxes of CO_2 on a global scale, and across southern, tropical, and northern latitudes to provide some broad geographical context. These values are broadly consistent with annual values for the atmospheric CO_2 growth rates – an important zeroth order assessment of our *a posteriori* net fluxes. Our value for 2023 inferred from OCO-2 data is 3.0 ppm/yr, about 0.2 ppm/yr higher than the value inferred from NOAA CO_2 mole fraction data. Building on ongoing our model evaluation, e.g., Deng et al., (2024) and Friedlingstein et al., (2024), we find that the *a posteriori* CO_2 concentrations for 2023 are generally within 0.5 ppm of data collected by spectrometers from the Total Carbon Column Observing Network (Wunch et al., 2011), with a standard deviation smaller than1.2 ppm.

As expected, the largest contribution of the global net flux originates from the northern hemisphere (Figure 2d), where there is a superposition of boreal and midlatitude ecosystems that contribute to the global uptake of CO_2 and large cities and other emission hotspots. At these latitudes, the year-to-year variations are comparatively small, limited to << 1PgC, and in the last two years since the 2021 peak there has been a small decrease in net emissions to pre-pandemic values (3.38—3.96 PgC/yr, 2014—2020). Over our study, these changes have typically represented 62—92% of the global budget, with the smallest

https://doi.org/10.5194/egusphere-2025-1793
Preprint. Discussion started: 6 May 2025

values typically during El Niño years when the tropics plays a larger role. The tropics show large year-to-year changes over our study period (Figure 2c) with a large peak in emissions that we have not observed since the 2015/2016 El Niño. We find the large increase in net CO_2 fluxes predominately originates from the tropics, representing 21% in 2022 and 38% in 2023. Our calculations suggest that this anomalous increase in tropical CO_2 flux in 2023 is explained mainly by an increased CO_2 flux over East Amazon (Figure A3). The net uptake in the southern hemisphere (Figure 2b) also shows a similar but small year-to-year change with the highest uptake in the last years, consequently compensating for emissions elsewhere on the globe. The 16% decrease in net uptake in 2023 reduced the influence of this region on the global net flux, reinforcing the role of the tropics on the global scale.

Figure 3 shows annual spatial distributions of the annual change in the net biosphere exchange (NBE) – the net CO_2 flux minus the *a priori* fossil fuel emissions removed – from 2022 to 2023 and as a comparison from 2014 to 2015 when there was a comparably largest change in the growth rate associated with the 2015/2015 El Niño. This widely used subtraction approach to determine NBE implicitly assumes perfect knowledge of fossil fuel combustion of CO_2, but we acknowledge that making that assumption has implications for NBE estimates, although this is minimal over the tropics where anthropogenic emissions are comparatively small (Oda et al., 2023). A positive annual change in NBE represents a larger net amount of CO_2 to the atmosphere. We find that the largest positive increases in NBE are found across the tropics, with peak values over eastern Brazil, southern Africa, eastern and southern China, mainland and maritime Southeast Asia, and Southeast Australia. The emission hotspot over western Canada is from wildfires (Byrne et al., 2024) but our *a posteriori* feature is almost exclusively from the *a priori* inventory, determined by independent satellite data, because large aerosol optical depths over and downwind of these extensive fires where OCO-2 data are unreliable; Byrne et al., (2024) inferred carbon emissions from these fires using satellite observations of carbon monoxide. We also find large positive increases in MBE over Alaska and Russia. Regions with elevated uptake in 2023 are limited to the US and central Canada, mainland Europe, with weaker uptake over Siberia, Turkey, and some parts of East Africa. In comparison, the tropics in 2015 shows regions with positive and negative changes in NBE over tropical South America, a large increase over East and Central Africa (Palmer et al., 2019), with some of the largest increases over mainland and maritime Southeast Asia, as we also found in 2023. Elevated uptake was mainly confined to boreal latitudes. These changes in *a posteriori* fluxes are broadly consistent with independent estimates of GPP changes inferred from the OCO-2 SIF data product and from vegetation greenness, providing us with some confidence that our estimated fluxes are physically plausible. The annual mean budgets for individual geographical regions where we see the largest changes in NBE (rectangles in Figure 3a), show that East Amazon is almost exclusively responsible for the large increase in pan-tropical CO_2 flux in 2023, with a smaller contribution from Southeast Asia.

Figure 4 shows the geographical distribution of changes in parameters that describe large-scale changes CO_2 fluxes – temperature and water availability. Geographical locations where we report the largest increases in NBE (and largest

https://doi.org/10.5194/egusphere-2025-1793
Preprint. Discussion started: 6 May 2025

reductions in GPP) in 2023, e.g., Brazil, southern Africa, southeast Australia, are coincident with locations where we saw some of the largest increases in temperature, VPD, and the largest reductions in LWE. And where we reported the largest decreases in NBE (and largest increases in GPP), e.g. parts of the contiguous US and central Canada, we saw cooler temperatures and lower VPDs, and small increases in LWE. We find a similar level of consistency between the data products and meteorological reanalyses in 2015.

Figure 5 describes these relationships more quantitatively by using linear and quadratic multivariate fits of MERRA2 rainfall, temperature, and soil moisture anomalies to our *a posteriori* NBE anomalies over the geographical regions highlighted in Figure 3a. In sensitivity calculations, we find that changes in VPD or LWE do not improve the fits to NBE anomalies. We find the quadratic fit marginally outperforms the linear fit but for simplicity of interpretation we use the linear fits, with both models being significantly significant, with p values < 0.001. The models capture most of the NBE changes, with the notable exception of mid 2022 when our NBE fluxes shows a sharp increase that is not explained by temperature or water. Based on the normalized linear fitting coefficients, we find for these fits that changes in temperature explain most of the NBE changes we observe over East Amazon (Table A1), but soil moisture changes are more important over Northern tropical Africa, southern Africa, and tropical Asia. Rainfall changes are more important over Southeast Asia. Independent GOSIF GPP estimates determined from satellite SIF observations (Li and Xiao, 2019) show a significant decrease from 2022 to 2023 over tropical regions, particularly over eastern Amazonia, southern Africa, tropical Asia and Southeast Asia (Figure A4), consistent with the increase we report for our *a posteriori* NBE estimates (Figure 5). More generally, we find that changes in GOSIF GPP are better than other individual predictors at describing our *a posteriori* CO_2 flux anomalies over Tropical Asia, Southeast Asia, and southern Africa (Table A2), 2014—2023, inclusively.

4 Concluding Remarks

We reported regional changes in the net biospheric exchange (NBE) of CO_2 inferred from OCO-2 retrievals of XCO2 from 2022 and 2023 to examine the origin of the large atmospheric growth rate reported for that period. Positive values of NBE denote net CO_2 fluxes to the atmosphere. We find that most of the increase in atmospheric CO_2 in 2023 is due to increased NBE over the land tropics, supported by a modest reduction in uptake in southern extratropics, in agreement with a recent study (Gui et al., 2024). Further examination revealed foci of increased NBE were over eastern Brazil, southern Africa, eastern and southern China, mainland and maritime Southeast Asia, and Southeast Australia. Extensive wildfires over western Canada during boreal summer months also substantially contributed to the atmospheric CO_2 growth rate in 2023 (Byrne et al., 2024), but in terms of atmospheric CO_2 this information is exclusively from the *a priori* inventory that is determined by independent satellite data. We also find increased uptake (lower NBE values) over the US and central Canada, mainland Europe, with weaker uptake over Siberia, Turkey, and some parts of East Africa. These large-scale patterns of NBE are consistent with data-driven estimates of gross primary production and vegetation greenness, and with changes in

https://doi.org/10.5194/egusphere-2025-1793
Preprint. Discussion started: 6 May 2025

surface temperature, rainfall, and surface water. We find that warmer temperatures in 2023 explain most of the change in NBE over eastern Brazil, with changes in hydrological quantities – rainfall or soil moisture – more important elsewhere across the tropics. Additional knowledge is needed to help reconcile CO_2 flux estimates from land biosphere process-based models and those inferred from inversions (Kondo et al., 2020). Our quantitative exploration of the relationships between our *a posteriori* NBE anomalies and changes in environmental parameter helps to interpret observed changes in atmospheric CO_2 but can also help to evaluate and improve process-based land biosphere models.

Our analysis has focused on 2023, but it is important to put this one year into a broader historical context, at least in the past decade when we have seen a marked increase in atmospheric growth rates of atmospheric CO_2 (Figure 1). Some of this increase can be explained by changes in fossil fuel combustion and other forms of human activity, but the largest spikes in atmospheric CO_2 growth rates coincide with years when there is a strong El Niño event (Figure 1), primarily associated with large-scale perturbations to the hydrological cycle that impact tropical ecosystems. In strong El Niño years, such as 2015/2016, widespread droughts reported across the tropics (Jiménez-Muñoz et al., 2016) resulted in a notable increase in fires (Liu et al., 2017) and can in some ecosystems lead to a widespread loss of tree density and a change the floristic composition (Prestes et al., 2024).

In 2023, the multivariate El Niño Southern Oscillation index, indicative of El Niño and La Niña strength, in 2023 was approximately half the value of recent El Niño events, such as 2015/2016. There are distinct differences in the spatial patterns of rainfall, atmospheric aridity (given by vapour pressure deficit), and soil moisture over the tropics (Figure 4). But the loss of carbon sequestration in 2023 and 2015/2016 was comparable. Our findings highlight the complex response of the tropical biosphere to environmental change, reflecting differences in the sensitivity and vulnerability of plants to localized droughts and increasing surface temperature (Table A1). Further quantifying these different sensitivities using independent *in situ* ecological observations will significantly improve our ability to model important biospheric processes in terms of atmospheric-biosphere carbon exchange, e.g., Liu et al., (2024).

Our interpretation of the OCO-2 column data suggests that the reduced uptake of CO_2 from tropical ecosystems played a key role in determining the anomalously large atmospheric CO_2 growth rates in 2023. Our work is largely consistent with a recent independent study (Gui et al., 2024) that used the same OCO-2 data, but interpreted them with an independent atmospheric transport model, driven by different fossil fuel inventories and by AI-based dynamic global vegetation models. They also used a different inverse method approach. However, our results and those reported by Gui et al., (2024) are inconsistent with another independent study (Ke et al., 2024), based on a set of land biosphere models and an inversion experiment from the Copernicus Atmosphere Monitoring Service (CAMS). They significantly differ in the spatial patterns of carbon release and uptake. Resolving these discrepancies is beyond the scope of this work, but ultimately they do need to be resolved if we are to use these models to predict how global ecosystems will respond to a warming climate and an accelerated hydrological cycle, and the subsequent impacts on the carbon cycle (Armstrong McKay et al., 2022). If our main result is accurate – a moderate El Niño event has led to a significant reduction in carbon uptake by the tropical land biosphere, which has experienced extensive drought – we might be observing the beginning of a decline in the ability of tropical ecosystems to absorb carbon. The long-term nature of this situation is unclear without further data, although the preliminary estimate of the 2024 atmospheric CO_2 growth rate of 3.75±0.08 ppm/yr is unprecedented since these records began in the late 1950s (https://gml.noaa.gov/ccgg/trends/gl_gr.html; last access: 15th April 2025). A coordinated measurement campaign is urgently needed to document how tropical ecosystems are changing, whether these changes compromise the future ability to absorb and store carbon, and whether prolonged drought will substantially delay any ecosystem recovery.

Regularly reporting regional CO_2 fluxes with minimal delay, and interpreting them using auxiliary data, e.g., related to fire (such as the extensive North American boreal forest fires in 2023) and hydrology, are enabled by massive-scale international investment in satellite instruments that complement the detailed information provided by ground-based measurement networks. Collectively, these efforts provide vast volumes of information about the state of the planet at a time when we are observing unprecedented environmental changes. These data and the analysis tools needed to infer CO_2 fluxes collectively represent an invaluable scientific resource that must be used to deliver frequent actionable information for policy makers. The agreement and divergence between our results and those from other independent studies underscore the efficacy and the shortcomings of the prevailing frameworks.

Code Availability

The community-led GEOS-Chem model of atmospheric chemistry and transport model is maintained centrally by Harvard University (https://geoschem.github.io/, last access: 5 May 2025), and is available on request. The ensemble Kalman filter code is publicly available as PyOSSE (https://www.nceo.ac.uk/data-facilities/datasets-tools/?dataset_type=tools, NCEO, last access: 5 May 2025).

Data Availability

The L2 column carbon dioxide data from OCO-2 and OCO-3 are available from the Goddard Earth Sciences Data and Information Services Centre (https://doi.org/10.5067/E4E140XDMPO2; last access 5 May 2025). The GOSIF GPP is available for public from https://data.globalecology.unh.edu/data/GOSIF-GPP_v2 (last access 5 May 2025). The MODIS EVI of version v06.1 is available from https://lpdaac.usgs.gov/products/myd13a3v061/ (last access 5 May 2025).

Author contributions

LF and PIP designed the research with contributions from LS; LF prepared the calculations; PIP and LF wrote the paper; JX, PC, AL, OH, RK, SM, SMP, XR, and MS provided data and comments on the manuscript.

https://doi.org/10.5194/egusphere-2025-1793
Preprint. Discussion started: 6 May 2025

Competing interests

None of the authors has any competing interests.

Acknowledgements

We gratefully acknowledge science teams of the NASA Orbiting Carbon Observatory. We also thank the GEOS-Chem community, particularly the team at Harvard University who helped to maintain the GEOS-Chem model, and the NASA Global Modeling and Assimilation Office (GMAO) who provided the MERRA2 data product.

Financial support

PIP and LF received support from the UK National Centre for Earth Observation funded by the Natural Environment Research Council (grant no. NE/R016518/1) and from the UK Space Agency. JX. was supported by the National Science Foundation (Macrosystem Biology & NEON-Enabled Science program: DEB-2017870) and the Iola Hubbard Climate Change Endowment. XR is funded by The National Institute of Standards and Technology, USA (#70NANB18H16). ICOS activities at CMN are supported by the JRU-ICOS Italy and by Project ITINERIS – Italian Integrated Environmental Research Infrastructures System (Project code IR0000032) within PIANO NAZIONALE DI RIPRESA E RESILIENZA, MISSIONE 4, COMPONENTE 2, INVESTIMENTO 3.1 "Fondo per la realizzazione di un sistema integrato di infrastrutture di ricerca e innovazione", which also supports the Simonetta Montaguti's position. Measurements at Jungfraujoch were supported by ICOS Switzerland (SNF grant 20F120_198227).

References

Ainsworth, E. A. and Rogers, A.: The response of photosynthesis and stomatal conductance to rising [CO_2]: mechanisms and environmental interactions, Plant Cell & Environment, 30, 258–270, https://doi.org/10.1111/j.1365-3040.2007.01641.x, 2007.

Armstrong McKay, D. I., Staal, A., Abrams, J. F., Winkelmann, R., Sakschewski, B., Loriani, S., Fetzer, I., Cornell, S. E., Rockström, J., and Lenton, T. M.: Exceeding 1.5°C global warming could trigger multiple climate tipping points, Science, 377, eabn7950, https://doi.org/10.1126/science.abn7950, 2022.

Baker, D. F., Law, R. M., Gurney, K. R., Rayner, P., Peylin, P., Denning, A. S., Bousquet, P., Bruhwiler, L., Chen, Y. -H., Ciais, P., Fung, I. Y., Heimann, M., John, J., Maki, T., Maksyutov, S., Masarie, K., Prather, M., Pak, B., Taguchi, S., and Zhu, Z.: TransCom 3 inversion intercomparison: Impact of transport model errors on the interannual variability of regional CO_2 fluxes, 1988–2003, Global Biogeochemical Cycles, 20, 2004GB002439, https://doi.org/10.1029/2004GB002439, 2006.

Barlow, J. M., Palmer, P. I., Bruhwiler, L. M., and Tans, P.: Analysis of CO_2 mole fraction data: first evidence of large-scale changes in CO_2 uptake at high northern latitudes, Atmos. Chem. Phys., 15, 13739–13758, https://doi.org/10.5194/acp-15-13739-2015, 2015.

https://doi.org/10.5194/egusphere-2025-1793
Preprint. Discussion started: 6 May 2025

Basso, L. S., Wilson, C., Chipperfield, M. P., Tejada, G., Cassol, H. L. G., Arai, E., Williams, M., Smallman, T. L., Peters, W., Naus, S., Miller, J. B., and Gloor, M.: Atmospheric CO_2 inversion reveals the Amazon as a minor carbon source caused by fire emissions, with forest uptake offsetting about half of these emissions, Atmos. Chem. Phys., 23, 9685–9723, https://doi.org/10.5194/acp-23-9685-2023, 2023.

Bennett, B. F., Salawitch, R. J., McBride, L. A., Hope, A. P., and Tribett, W. R.: Quantification of the Airborne Fraction of Atmospheric CO_2 Reveals Stability in Global Carbon Sinks Over the Past Six Decades, JGR Biogeosciences, 129, e2023JG007760, https://doi.org/10.1029/2023JG007760, 2024.

Bettadpur, S.: CSR Level-2 Processing Standards Document for Product Release 04. GRACE, 2007.

Buermann, W., Lintner, B. R., Koven, C. D., Angert, A., Pinzon, J. E., Tucker, C. J., and Fung, I. Y.: The changing carbon cycle at Mauna Loa Observatory, Proc. Natl. Acad. Sci. U.S.A., 104, 4249–4254, https://doi.org/10.1073/pnas.0611224104, 2007.

Byrne, B., Liu, J., Bowman, K. W., Pascolini-Campbell, M., Chatterjee, A., Pandey, S., Miyazaki, K., Van Der Werf, G. R., Wunch, D., Wennberg, P. O., Roehl, C. M., and Sinha, S.: Carbon emissions from the 2023 Canadian wildfires, Nature, 633, 835–839, https://doi.org/10.1038/s41586-024-07878-z, 2024.

Chatterjee, A., Gierach, M. M., Sutton, A. J., Feely, R. A., Crisp, D., Eldering, A., Gunson, M. R., O'Dell, C. W., Stephens, B. B., and Schimel, D. S.: Influence of El Niño on atmospheric CO_2 over the tropical Pacific Ocean: Findings from NASA's OCO-2 mission, Science, 358, eaam5776, https://doi.org/10.1126/science.aam5776, 2017.

Deng, Z., Ciais, P., Hu, L., Martinez, A., Saunois, M., Thompson, R. L., Tibrewal, K., Peters, W., Byrne, B., Grassi, G., Palmer, P. I., Luijkx, I. T., Liu, Z., Liu, J., Fang, X., Wang, T., Tian, H., Tanaka, K., Bastos, A., Sitch, S., Poulter, B., Albergel, C., Tsuruta, A., Maksyutov, S., Janardanan, R., Niwa, Y., Zheng, B., Thanwerdas, J., Belikov, D., Segers, A., and Chevallier, F.: Global Greenhouse Gas Reconciliation 2022, https://doi.org/10.5194/essd-2024-103, 5 July 2024.

Fang, Z., Zhang, W., Brandt, M., Abdi, A. M., and Fensholt, R.: Globally Increasing Atmospheric Aridity Over the 21st Century, Earth's Future, 10, e2022EF003019, https://doi.org/10.1029/2022EF003019, 2022.

Feng, L., Palmer, P. I., Bösch, H., and Dance, S.: Estimating surface CO_2 fluxes from space-borne CO_2 dry air mole fraction observations using an ensemble Kalman Filter, Atmospheric Chemistry and Physics, 9, 2619–2633, https://doi.org/10.5194/acp-9-2619-2009, 2009.

Feng, L., Palmer, P. I., Bösch, H., Parker, R. J., Webb, A. J., Correia, C. S. C., Deutscher, N. M., Domingues, L. G., Feist, D. G., Gatti, L. V., and Others: Consistent regional fluxes of CH4 and CO2 inferred from GOSAT proxy XCH4: XCO2 retrievals, 2010--2014, Atmos. Chem. Phys, 17, 4781–4797, 2017.

Feng, L., Palmer, P. I., Zhu, S., Parker, R. J., and Liu, Y.: Tropical methane emissions explain large fraction of recent changes in global atmospheric methane growth rate, Nature Communications, 13, 1378, https://doi.org/10.1038/s41467-022-28989-z, 2022.

Feng, L., Palmer, P. I., Parker, R. J., Lunt, M. F., and Bösch, H.: Methane emissions are predominantly responsible for record-breaking atmospheric methane growth rates in 2020 and 2021, Atmos. Chem. Phys., 23, 4863–4880, https://doi.org/10.5194/acp-23-4863-2023, 2023.

Flechtner, F.: GRACE AOD1B product description document for product releases 01 to 04, 2007.

Friedlingstein, P., O'Sullivan, M., Jones, M. W., Andrew, R. M., Bakker, D. C. E., Hauck, J., Landschützer, P., Le Quéré, C., Luijkx, I. T., Peters, G. P., Peters, W., Pongratz, J., Schwingshackl, C., Sitch, S., Canadell, J. G., Ciais, P., Jackson, R. B., Alin, S. R., Anthoni, P., Barbero, L., Bates, N. R., Becker, M., Bellouin, N., Decharme, B., Bopp, L., Brasika, I. B. M., Cadule, P., Chamberlain, M. A., Chandra, N., Chau, T.-T.-T., Chevallier, F., Chini, L. P., Cronin, M., Dou, X., Enyo, K., Evans, W., Falk, S., Feely, R. A., Feng, L., Ford, D. J., Gasser, T., Ghattas, J., Gkritzalis, T., Grassi, G., Gregor, L., Gruber, N., Gürses, Ö., Harris, I., Hefner, M., Heinke, J., Houghton, R. A., Hurtt, G. C., Iida, Y., Ilyina, T., Jacobson, A. R., Jain, A., Jarníková, T., Jersild, A., Jiang, F., Jin, Z., Joos, F., Kato, E., Keeling, R. F., Kennedy, D., Klein Goldewijk, K., Knauer, J., Korsbakken, J. I., Körtzinger, A., Lan, X., Lefèvre, N., Li, H., Liu, J., Liu, Z., Ma, L., Marland, G., Mayot, N., McGuire, P. C., McKinley, G. A., Meyer, G., Morgan, E. J., Munro, D. R., Nakaoka, S.-I., Niwa, Y., O'Brien, K. M., Olsen, A., Omar, A. M., Ono, T., Paulsen, M., Pierrot, D., Pocock, K., Poulter, B., Powis, C. M., Rehder, G., Resplandy, L., Robertson, E., Rödenbeck, C., Rosan, T. M., Schwinger, J., Séférian, R., et al.: Global Carbon Budget 2023, Earth Syst. Sci. Data, 15, 5301–5369, https://doi.org/10.5194/essd-15-5301-2023, 2023.

Friedlingstein, P., O'Sullivan, M., Jones, M. W., Andrew, R. M., Hauck, J., Landschützer, P., Le Quéré, C., Li, H., Luijkx, I. T., Olsen, A., Peters, G. P., Peters, W., Pongratz, J., Schwingshackl, C., Sitch, S., Canadell, J. G., Ciais, P., Jackson, R. B., Alin, S. R., Arneth, A., Arora, V., Bates, N. R., Becker, M., Bellouin, N., Berghoff, C. F., Bittig, H. C., Bopp, L., Cadule, P., Campbell, K., Chamberlain, M. A., Chandra, N., Chevallier, F., Chini, L. P., Colligan, T., Decayeux, J., Djeutchouang, L., Dou, X., Duran Rojas, C., Enyo, K., Evans, W., Fay, A., Feely, R. A., Ford, D. J., Foster, A., Gasser, T., Gehlen, M., Gkritzalis, T., Grassi, G., Gregor, L., Gruber, N., Gürses, Ö., Harris, I., Hefner, M., Heinke, J., Hurtt, G. C., Iida, Y., Ilyina, T., Jacobson, A. R., Jain, A., Jarníková, T., Jersild, A., Jiang, F., Jin, Z., Kato, E., Keeling, R. F., Klein Goldewijk, K., Knauer, J., Korsbakken, J. I., Lauvset, S. K., Lefèvre, N., Liu, Z., Liu, J., Ma, L., Maksyutov, S., Marland, G., Mayot, N., McGuire, P., Metzl, N., Monacci, N. M., Morgan, E. J., Nakaoka, S.-I., Neill, C., Niwa, Y., Nützel, T., Olivier, L., Ono, T., Palmer, P. I., Pierrot, D., Qin, Z., Resplandy, L., Roobaert, A., Rosan, T. M., Rödenbeck, C., Schwinger, J., Smallman, T. L., Smith, S., Sospedra-Alfonso, R., Steinhoff, T., Sun, Q., et al.: Global Carbon Budget 2024, https://doi.org/10.5194/essd-2024-519, 13 November 2024.

Graven, H. D., Keeling, R. F., Piper, S. C., Patra, P. K., Stephens, B. B., Wofsy, S. C., Welp, L. R., Sweeney, C., Tans, P. P., Kelley, J. J., Daube, B. C., Kort, E. A., Santoni, G. W., and Bent, J. D.: Enhanced Seasonal Exchange of CO_2 by Northern Ecosystems Since 1960, Science, 341, 1085–1089, https://doi.org/10.1126/science.1239207, 2013.

Gui, Y., Wang, K., Jin, Z., Wang, H., Deng, H., Li, X., Tian, X., Wang, T., Chen, W., Wang, T., and Piao, S.: The decline in tropical land carbon sink drove high atmospheric CO_2 growth rate in 2023, National Science Review, 11, nwae365, https://doi.org/10.1093/nsr/nwae365, 2024.

Gurney, K. R., Law, R. M., Denning, A. S., Rayner, P. J., Baker, D., Bousquet, P., Bruhwiler, L., Chen, Y.-H., Ciais, P., Fan, S., Fung, I. Y., Gloor, M., Heimann, M., Higuchi, K., John, J., Maki, T., Maksyutov, S., Masarie, K., Peylin, P., Prather, M., Pak, B. C., Randerson, J., Sarmiento, J., Taguchi, S., Takahashi, T., and Yuen, C.-W.: Towards robust regional estimates of CO_2 sources and sinks using atmospheric transport models, Nature, 415, 626–630, https://doi.org/10.1038/415626a, 2002.

Gurney, K. R., Law, R. M., Denning, A. S., Rayner, P. J., Pak, B. C., Baker, D., Bousquet, P., Bruhwiler, L., Chen, Y.-H., Ciais, P., and others: Transcom 3 inversion intercomparison: Model mean results for the estimation of seasonal carbon sources and sinks, Global Biogeochemical Cycles, 18, 2004.

Hugelius, G., Ramage, J., Burke, E., Chatterjee, A., Smallman, T. L., Aalto, T., Bastos, A., Biasi, C., Canadell, J. G., Chandra, N., Chevallier, F., Ciais, P., Chang, J., Feng, L., Jones, M. W., Kleinen, T., Kuhn, M., Lauerwald, R., Liu, J., López-Blanco, E., Luijkx, I. T., Marushchak, M. E., Natali, S. M., Niwa, Y., Olefeldt, D., Palmer, P. I., Patra, P. K., Peters, W., Potter, S., Poulter, B., Rogers, B. M., Riley, W. J., Saunois, M., Schuur, E. A. G., Thompson, R. L., Treat, C., Tsuruta, A., Turetsky, M. R., Virkkala, A. -M., Voigt, C., Watts, J., Zhu, Q., and Zheng, B.: Permafrost Region Greenhouse Gas Budgets Suggest a Weak CO_2 Sink and CH_4 and N_2 O Sources, But Magnitudes Differ Between Top-Down and Bottom-Up Methods, Global Biogeochemical Cycles, 38, e2023GB007969, https://doi.org/10.1029/2023GB007969, 2024.

ICOS RI, Apadula, F., Biermann, T., Colomb, A., Conil, S., Couret, C., Cristofanelli, P., De Mazière, M., Delmotte, M., Di Lorio, T., Emmenegger, L., Forster, G., Frumau, A., Haszpra, L., Hatakka, J., Heliasz, M., Hensen, A., Hermansen, O., Hoheisel, A., Kneuer, T., Komínková, K., Kubistin, D., Larmanou, E., Laurent, O., Laurila, T., Lehner, I., Lehtinen, K., Leskinen, A., Leuenberger, M., Lindauer, M., Lopez, M., Lund Myhre, C., Lunder, C., Mammarella, I., Manca, G., Manning, A., Marek, M. V., Marklund, P., Meinhardt, F., Molnár, M., Müller-Williams, J., O'Doherty, S., Piacentino, S., Pichon, J.-M., Pitt, J., Platt, S. M., Plaß-Dülmer, C., Ramonet, M., Rivas-Soriano, P., Roulet, Y.-A., Scheeren, B., Schmidt, M., Sferlazzo, D., Sha, M. K., Stanley, K., Steinbacher, M., Sørensen, L. L., Trisolino, P., Vítková, G., Yver-Kwok, C., Zazzeri, G., di Sarra, A., ICOS ATC-Laboratoires des Sciences du Climat et de L'Environnement (LSCE), France, and ICOS Flask And Calibration Laboratory (FCL), Germany: ICOS Atmosphere 2024.3 FastTrack release of Level 1.5 Greenhouse Gas Mole Fractions of CO_2, CH_4, N_2O, CO and meteorology, https://doi.org/10.18160/S9BD-H5YY, 9 October 2024.

Jiménez-Muñoz, J. C., Mattar, C., Barichivich, J., Santamaría-Artigas, A., Takahashi, K., Malhi, Y., Sobrino, J. A., and Schrier, G. V. D.: Record-breaking warming and extreme drought in the Amazon rainforest during the course of El Niño 2015–2016, Sci Rep, 6, 33130, https://doi.org/10.1038/srep33130, 2016.

Ke, P., Ciais, P., Sitch, S., Li, W., Bastos, A., Liu, Z., Xu, Y., Gui, X., Bian, J., Goll, D. S., Xi, Y., Li, W., O'Sullivan, M., Goncalves De Souza, J., Friedlingstein, P., and Chevallier, F.: Low latency carbon budget analysis reveals a large decline of the land carbon sink in 2023, National Science Review, 11, nwae367, https://doi.org/10.1093/nsr/nwae367, 2024.

Keeling, C. D.: The Concentration and Isotopic Abundances of Carbon Dioxide in the Atmosphere, Tellus, 12, 200–203, https://doi.org/10.1111/j.2153-3490.1960.tb01300.x, 1960.

Keeling, C. D., Bacastow, R. B., Bainbridge, A. E., Ekdahl, C. A., Guenther, P. R., Waterman, L. S., and Chin, J. F. S.: Atmospheric carbon dioxide variations at Mauna Loa Observatory, Hawaii, Tellus A: Dynamic Meteorology and Oceanography, 28, 538, https://doi.org/10.3402/tellusa.v28i6.11322, 1976.

Keeling, C. D., Chin, J. F. S., and Whorf, T. P.: Increased activity of northern vegetation inferred from atmospheric CO2 measurements, Nature, 382, 146–149, https://doi.org/10.1038/382146a0, 1996.

Kondo, M., Patra, P. K., Sitch, S., Friedlingstein, P., Poulter, B., Chevallier, F., Ciais, P., Canadell, J. G., Bastos, A., Lauerwald, R., Calle, L., Ichii, K., Anthoni, P., Arneth, A., Haverd, V., Jain, A. K., Kato, E., Kautz, M., Law, R. M., Lienert, S., Lombardozzi, D., Maki, T., Nakamura, T., Peylin, P., Rödenbeck, C., Zhuravlev, R., Saeki, T., Tian, H., Zhu, D., and Ziehn, T.: State of the science in reconciling top-down and bottom-up approaches for terrestrial CO_2 budget, Global Change Biology, 26, 1068–1084, https://doi.org/10.1111/gcb.14917, 2020.

Li, X. and Xiao, J.: Mapping Photosynthesis Solely from Solar-Induced Chlorophyll Fluorescence: A Global, Fine-Resolution Dataset of Gross Primary Production Derived from OCO-2, Remote Sensing, 11, 2563, https://doi.org/10.3390/rs11212563, 2019.

Liu, J., Bowman, K. W., Schimel, D. S., Parazoo, N. C., Jiang, Z., Lee, M., Bloom, A. A., Wunch, D., Frankenberg, C., Sun, Y., O'Dell, C. W., Gurney, K. R., Menemenlis, D., Gierach, M., Crisp, D., and Eldering, A.: Contrasting carbon cycle responses of the tropical continents to the 2015-2016 El Niño, Science, 358, https://doi.org/10.1126/science.aam5690, 2017.

Liu, J., Bowman, K., Palmer, P. I., Joiner, J., Levine, P., Bloom, A. A., Feng, L., Saatchi, S., Keller, M., Longo, M., Schimel, D., and Wennberg, P. O.: Enhanced Carbon Flux Response to Atmospheric Aridity and Water Storage Deficit During the 2015–2016 El Niño Compromised Carbon Balance Recovery in Tropical South America, AGU Advances, 5, e2024AV001187, https://doi.org/10.1029/2024AV001187, 2024.

Oda, T. and Maksyutov, S.: ODIAC Fossil Fuel CO_2 Emissions Dataset (Version name: ODIAC2020b), https://doi.org/10.17595/20170411.001, 2021.

Oda, T., Maksyutov, S., and Andres, R. J.: The Open-source Data Inventory for Anthropogenic CO_2, version 2016 (ODIAC2016): a global monthly fossil fuel CO_2 gridded emissions data product for tracer transport simulations and surface flux inversions, Earth Syst. Sci. Data, 10, 87–107, https://doi.org/10.5194/essd-10-87-2018, 2018.

Oda, T., Feng, L., Palmer, P. I., Baker, D. F., and Ott, L. E.: Assumptions about prior fossil fuel inventories impact our ability to estimate posterior net CO_2 fluxes that are needed for verifying national inventories, Environ. Res. Lett., 18, 124030, https://doi.org/10.1088/1748-9326/ad059b, 2023.

Olsen, S. C. and Randerson, J. T.: Differences between surface and column atmospheric CO_2 and implications for carbon cycle research, J. Geophys. Res., 109, 2003JD003968, https://doi.org/10.1029/2003JD003968, 2004.

O'Sullivan, M., Sitch, S., Friedlingstein, P., Luijkx, I. T., Peters, W., Rosan, T. M., Arneth, A., Arora, V. K., Chandra, N., Chevallier, F., Ciais, P., Falk, S., Feng, L., Gasser, T., Houghton, R. A., Jain, A. K., Kato, E., Kennedy, D., Knauer, J., McGrath, M. J., Niwa, Y., Palmer, P. I., Patra, P. K., Pongratz, J., Poulter, B., Rödenbeck, C., Schwingshackl, C., Sun, Q., Tian, H., Walker, A. P., Yang, D., Yuan, W., Yue, X., and Zaehle, S.: The key role of forest disturbance in reconciling estimates of the northern carbon sink, Commun Earth Environ, 5, 705, https://doi.org/10.1038/s43247-024-01827-4, 2024.

Page, S. E., Siegert, F., Rieley, J. O., Boehm, H.-D. V., Jaya, A., and Limin, S.: The amount of carbon released from peat and forest fires in Indonesia during 1997, Nature, 420, 61–65, https://doi.org/10.1038/nature01131, 2002.

Palmer, P. I., Feng, L., Baker, D., Chevallier, F., Bösch, H., and Somkuti, P.: Net carbon emissions from African biosphere dominate pan-tropical atmospheric CO_2 signal, Nature Communications, 10, 3344–3344, https://doi.org/10.1038/s41467-019-11097-w, 2019.

Patra, P. K., Crisp, D., Kaiser, J. W., Wunch, D., Saeki, T., Ichii, K., Sekiya, T., Wennberg, P. O., Feist, D. G., Pollard, D. F., Griffith, D. W. T., Velazco, V. A., De Maziere, M., Sha, M. K., Roehl, C., Chatterjee, A., and Ishijima, K.: The Orbiting Carbon Observatory (OCO-2) tracks 2–3 peta-gram increase in carbon release to the atmosphere during the 2014–2016 El Niño, Sci Rep, 7, 13567, https://doi.org/10.1038/s41598-017-13459-0, 2017.

Prestes, N. C. C. S., Marimon, B. S., Morandi, P. S., Reis, S. M., Junior, B. H. M., Cruz, W. J. A., Oliveira, E. A., Mariano, L. H., Elias, F., Santos, D. M., Esquivel-Muelbert, A., and Phillips, O. L.: Impact of the extreme 2015-16 El Niño climate event on forest and savanna tree species of the Amazonia-Cerrado transition, Flora, 319, 152597, https://doi.org/10.1016/j.flora.2024.152597, 2024.

Randerson, J. T., Van der Werf, G. R., Giglio, L., Collatz, G. J., and Kasibhatla, P. S.: Global Fire Emissions Database, Version 4.1 (GFEDv4), 1925.7122549999906 MB, https://doi.org/10.3334/ORNLDAAC/1293, 2017.

Schuh, A. E., Jacobson, A. R., Basu, S., Weir, B., Baker, D., Bowman, K., Chevallier, F., Crowell, S., Davis, K. J., Deng, F., Denning, S., Feng, L., Jones, D., Liu, J., and Palmer, P. I.: Quantifying the Impact of Atmospheric Transport Uncertainty on CO_2 Surface Flux Estimates, Global Biogeochemical Cycles, 33, 484–500, https://doi.org/10.1029/2018GB006086, 2019.

Schuldt, K. N., Mund, J., Luijkx, I. T., Aalto, T., Abshire, J. B., Aikin, K., Arlyn Andrews, Aoki, S., Apadula, F., Baier, B., Bakwin, P., Bartyzel, J., Bentz, G., Bergamaschi, P., Beyersdorf, A., Biermann, T., Biraud, S. C., Boenisch, H., Bowling, D., Brailsford, G., Brand, W. A., Van Den Bulk, P., Chen, G., Huilin Chen, Lukasz Chmura, Clark, S., Sites Climadat, Coletta, J. D., Colomb, A., Commane, R., Conil, S., Couret, C., Cox, A., Cristofanelli, P., Cuevas, E., Curcoll, R., Daube, B., Davis, K., Delmotte, M., DiGangi, J. P., Van Dinther, D., Dlugokencky, E., Elkins, J. W., Emmenegger, L., Shuangxi Fang, Fischer, M. L., Forster, G., Frumau, A., Galkowski, M., Gatti, L. V., Gehrlein, T., Gerbig, C., Francois Gheusi, Gloor, E., Gomez-Trueba, V., Goto, D., Griffis, T., Hammer, S., Hanson, C., Haszpra, L., Hatakka, J., Heimann, M., Heimann, M., Heliasz, M., Heltai, D., Hensen, A., Hermanssen, O., Hintsa, E., Hoheisel, A., Holst, J., Ivakhov, V., Jaffe, D., Jordan, A., Joubert, W., Karion, A., Kawa, S. R., Kazan, V., Keeling, R., Keronen, P., Jooil Kim, Kneuer, T., Kolari, P., Kominkova, K., Kort, E., Kozlova, E., Krummel, P., Kubistin, D., Labuschagne, C., Lam, D. H. Y., Lan, X., Langenfelds, R., Laurent, O., Laurila, T., Lauvaux, T., Lavric, J., Law, B., Lee, J., Lee, O. S. M., Lehner, I., et al.: Multi-laboratory compilation of atmospheric carbon dioxide data for the period 1957-2021; obspack_co2_1_GLOBALVIEWplus_v8.0_2022-08-27, https://doi.org/10.25925/20220808, 2022.

Takahashi, T., Sutherland, S. C., Wanninkhof, R., Sweeney, C., Feely, R. A., Chipman, D. W., Hales, B., Friederich, G., Chavez, F., Sabine, C., Watson, A., Bakker, D. C. E., Schuster, U., Metzl, N., Yoshikawa-Inoue, H., Ishii, M., Midorikawa, T., Nojiri, Y., Körtzinger, A., Steinhoff, T., Hoppema, M., Olafsson, J., Arnarson, T. S., Tilbrook, B., Johannessen, T., Olsen, A., Bellerby, R., Wong, C. S., Delille, B., Bates, N. R., and de Baar, H. J. W.: Climatological mean and decadal change in surface ocean pCO2, and net sea-air CO_2 flux over the global oceans, Deep-Sea Research Part II: Topical Studies in Oceanography, 56, https://doi.org/10.1016/j.dsr2.2008.12.009, 2009.

Tans, P. P., Fung, I. Y., and Takahashi, T.: Observational Constraints on the Global Atmospheric CO_2 Budget, Science, 247, 1431–1438, https://doi.org/10.1126/science.247.4949.1431, 1990.

Tapley, B. D., Bettadpur, S., Watkins, M., and Reigber, C.: The Gravity Recovery And Climate Experiment: Mission overview and early results, Geophysical Research Letters, 31, https://doi.org/10.1029/2004GL019920, 2004.

Taylor, T. E., O'Dell, C. W., Baker, D., Bruegge, C., Chang, A., Chapsky, L., Chatterjee, A., Cheng, C., Chevallier, F., Crisp, D., Dang, L., Drouin, B., Eldering, A., Feng, L., Fisher, B., Fu, D., Gunson, M., Haemmerle, V., Keller, G. R., Kiel, M., Kuai, L., Kurosu, T., Lambert, A., Laughner, J., Lee, R., Liu, J., Mandrake, L., Marchetti, Y., McGarragh, G., Merrelli, A., Nelson, R. R., Osterman, G., Oyafuso, F., Palmer, P. I., Payne, V. H., Rosenberg, R., Somkuti, P., Spiers, G., To, C., Weir, B., Wennberg, P. O., Yu, S., and Zong, J.: Evaluating the consistency between OCO-2 and OCO-3 XCO_2 estimates derived from the NASA ACOS version 10 retrieval algorithm, Atmos. Meas. Tech., 16, 3173–3209, https://doi.org/10.5194/amt-16-3173-2023, 2023.

Wang, J., Feng, L., Palmer, P. I., Liu, Y., Fang, S., Bösch, H., O'Dell, C. W., Tang, X., Yang, D., Liu, L., and Xia, C.: Large Chinese land carbon sink estimated from atmospheric carbon dioxide data, Nature, 586, 720–723, https://doi.org/10.1038/s41586-020-2849-9, 2020.

Wunch, D., Toon, G. C., Blavier, J.-F. L., Washenfelder, R. A., Notholt, J., Connor, B. J., Griffith, D. W. T., Sherlock, V., and Wennberg, P. O.: The Total Carbon Column Observing Network, Phil. Trans. R. Soc. A., 369, 2087–2112, https://doi.org/10.1098/rsta.2010.0240, 2011.

https://doi.org/10.5194/egusphere-2025-1793
Preprint. Discussion started: 6 May 2025

Figures

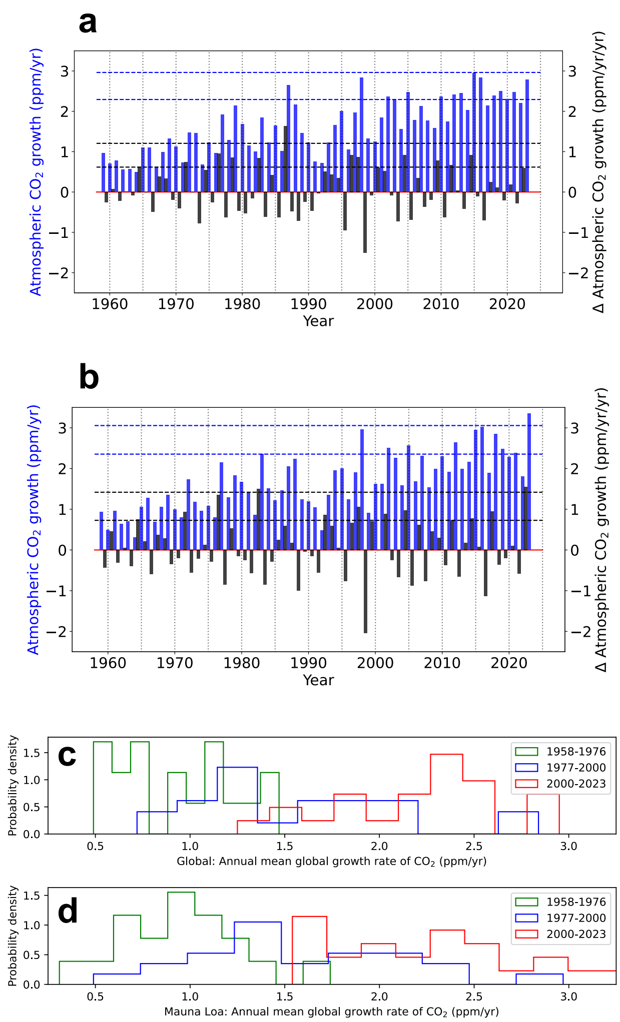

Figure 1 Atmospheric growth rates of CO_2 (blue) and their annual change (black). **a** Global mean values. **b** Values determined from Mauna Loa, Hawaii CO_2 mole fraction data. Data collected by NOAA and available at https://gml.noaa.gov/ccgg/trends/gl_gr.html. **c** Multi-decadal changes in the probability density of global mean annual mean growth rates and **d** as panel c but using data from Mauna Loa. Blue and black horizontal dashed lines denote the 1-σ and 2-σ values for the annual atmospheric CO_2 growth and its annual change, respectively.

https://doi.org/10.5194/egusphere-2025-1793
Preprint. Discussion started: 6 May 2025

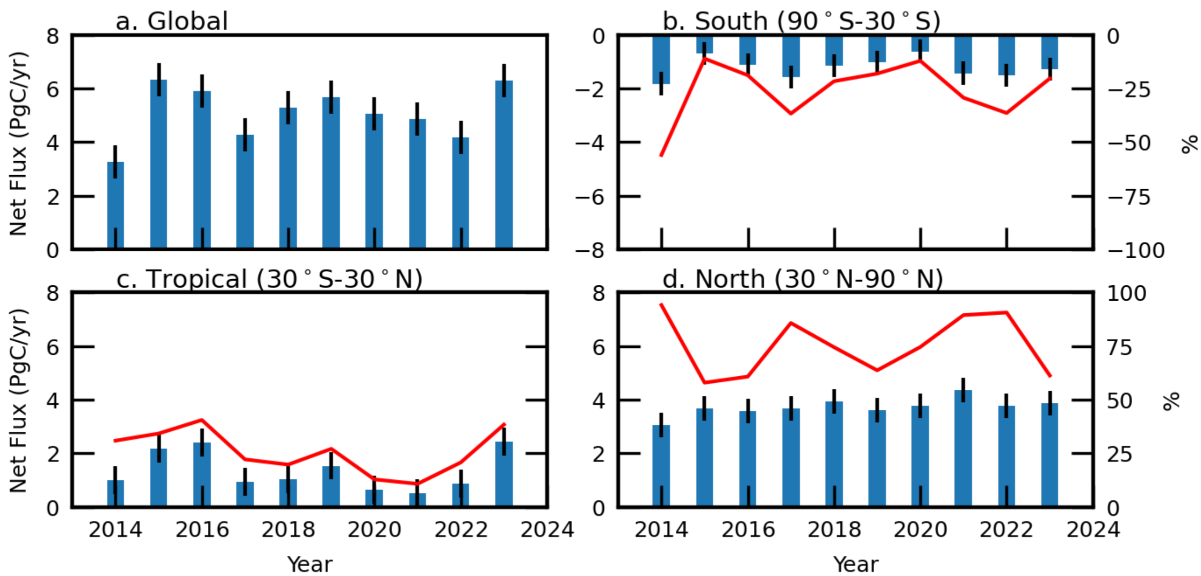

Figure 2 Annual mean *a posteriori* CO_2 flux estimates inferred from OCO-2 data for the globe, the southern extratropics, the tropics, and the northern extratropics. The thin black vertical lines denote the 1-sigma values about the annual mean values.
530 The red lines in panels b-d denote the percentage contribution to the global net fluxes.

https://doi.org/10.5194/egusphere-2025-1793
Preprint. Discussion started: 6 May 2025

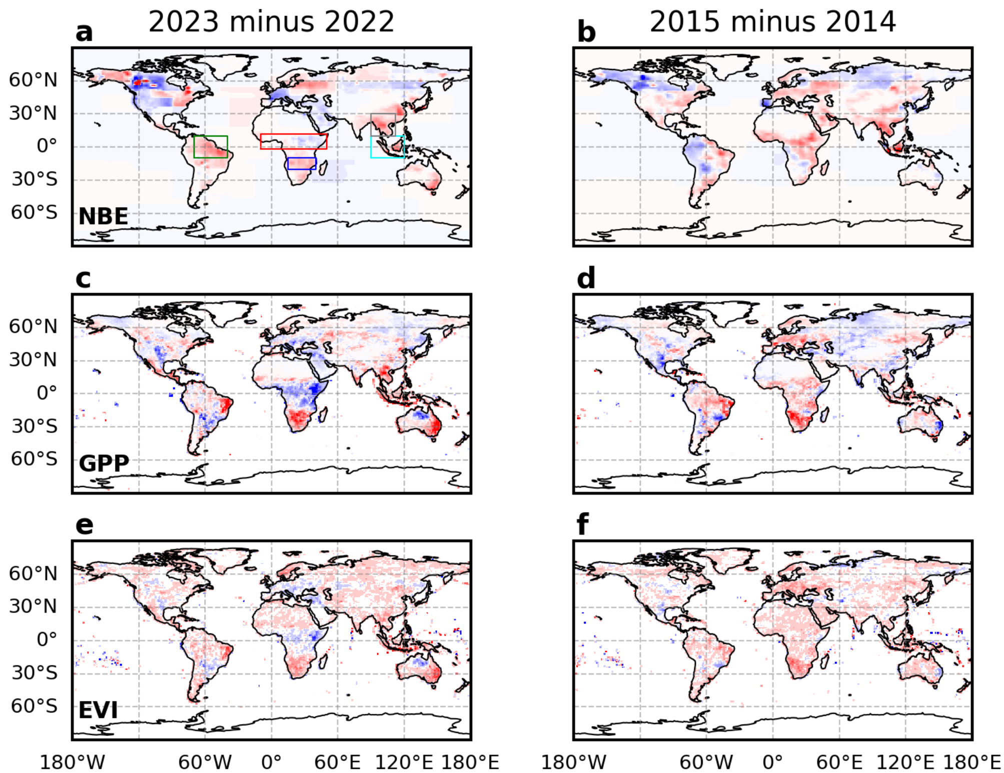

Figure 3 Differences in *a posteriori* CO_2 flux estimates inferred from OCO-2 data (top), gross primary production (GPP) estimated from OCO-2 SIF data (middle), and elevated vegetation indices (EVI) inferred from MODIS data (bottom) for
535 2022-2023 (left panels) and 2014-2015 (right panels). Rectangles shown in panel a describe the geographical regions we focus on for our multivariate fits.

https://doi.org/10.5194/egusphere-2025-1793
Preprint. Discussion started: 6 May 2025

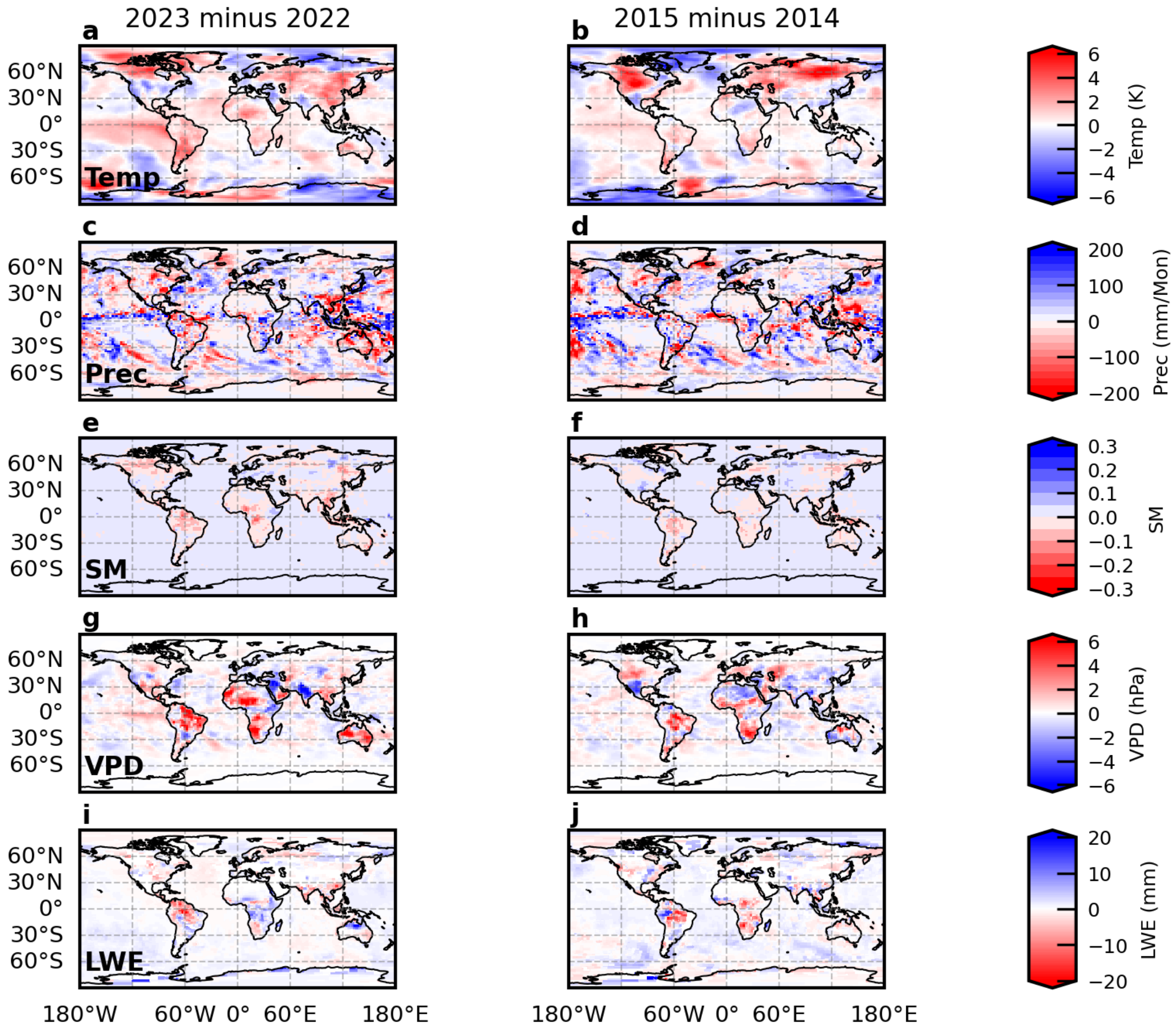

Figure 4 Differences in surface temperature (Temp; top row), precipitation (Prec; second row), soil moisture (SM; third row), vapour pressure deficit (VPD; fourth row), derived from soil moisture, based on MERRA2 reanalyses data products from NASA GSFC GMAO, and liquid water equivalent (LWE; bottom row) from the GRACE satellites for 2023 minus 2022 (left panels) and 2015 minus 2014 (right panels).

https://doi.org/10.5194/egusphere-2025-1793
Preprint. Discussion started: 6 May 2025

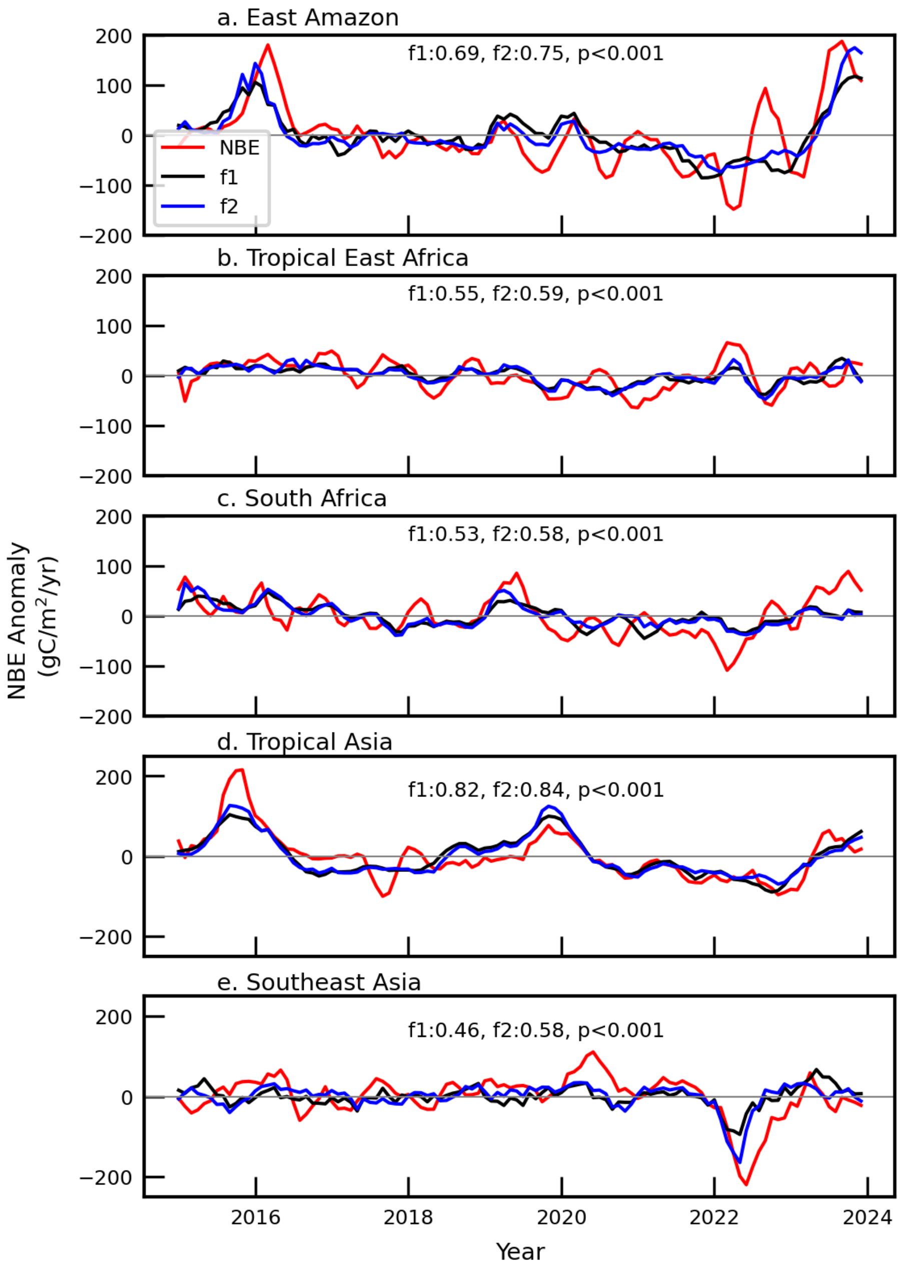

Figure 5 Regional linear (black) and quadratic (blue) multivariate fits of NBE anomalies (red) inferred from OCO-2 data using independent estimates of rainfall, surface temperature, and soil moisture from MERRA reanalyses data products from
545 NASA GSFC GMAO. Regional definitions, defined in panel a of Figure 3, include East Amazon, tropical East Africa, southern Africa, tropical Asian, and Southeast Asia. Number shown inset of each panel include the Pearson correlation coefficient for each fit, and the p-value that corresponds to both fits.

https://doi.org/10.5194/egusphere-2025-1793
Preprint. Discussion started: 6 May 2025

Appendix A

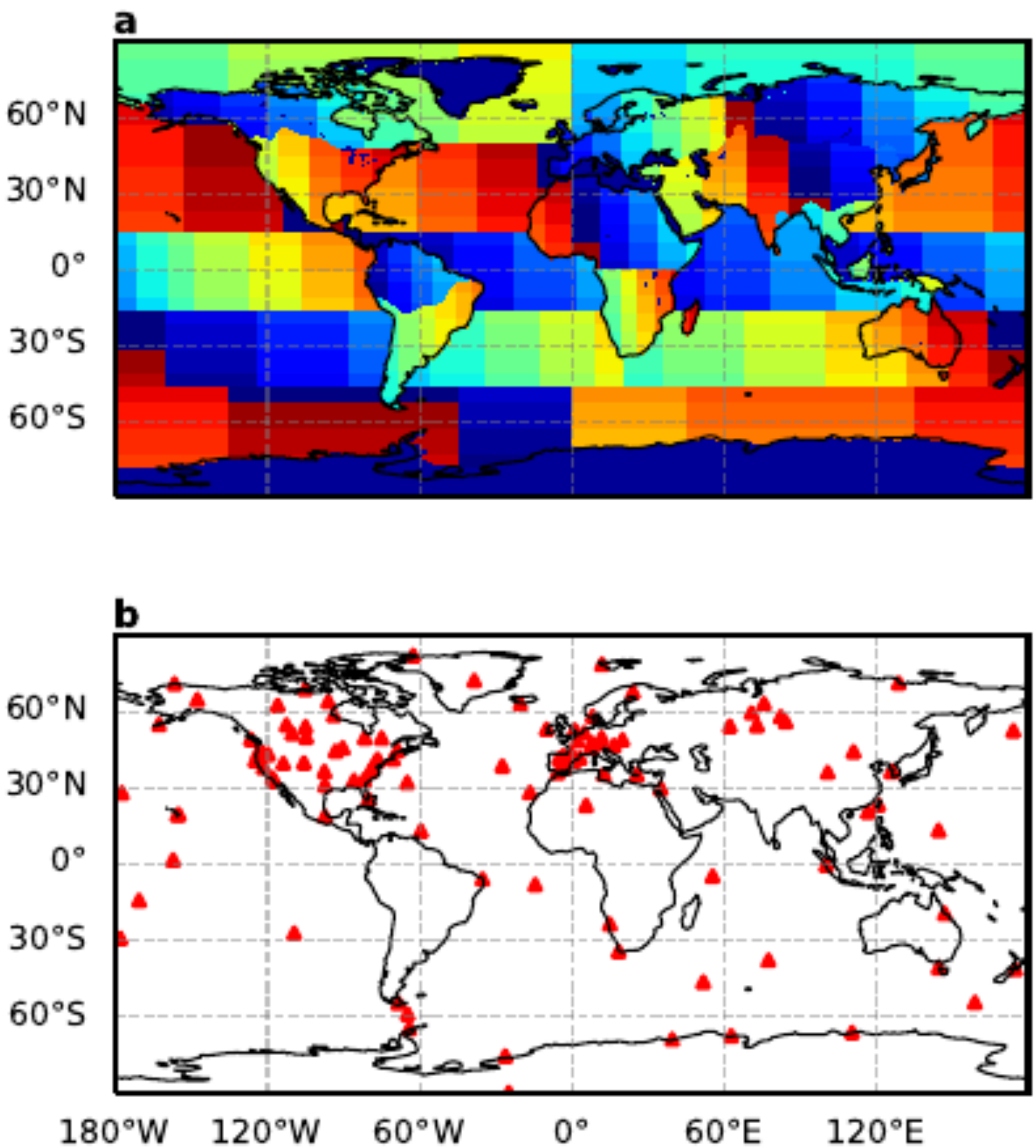

550 **Figure A1 a** The distribution of 488 sub-regions – including 356 land regions and 132 oceanic regions – for which we report monthly a posteriori CO2 flux estimates inferred from OCO-2 data. **b** The geographical locations of the ground-based measurements of CO2 mole fraction.

https://doi.org/10.5194/egusphere-2025-1793
Preprint. Discussion started: 6 May 2025

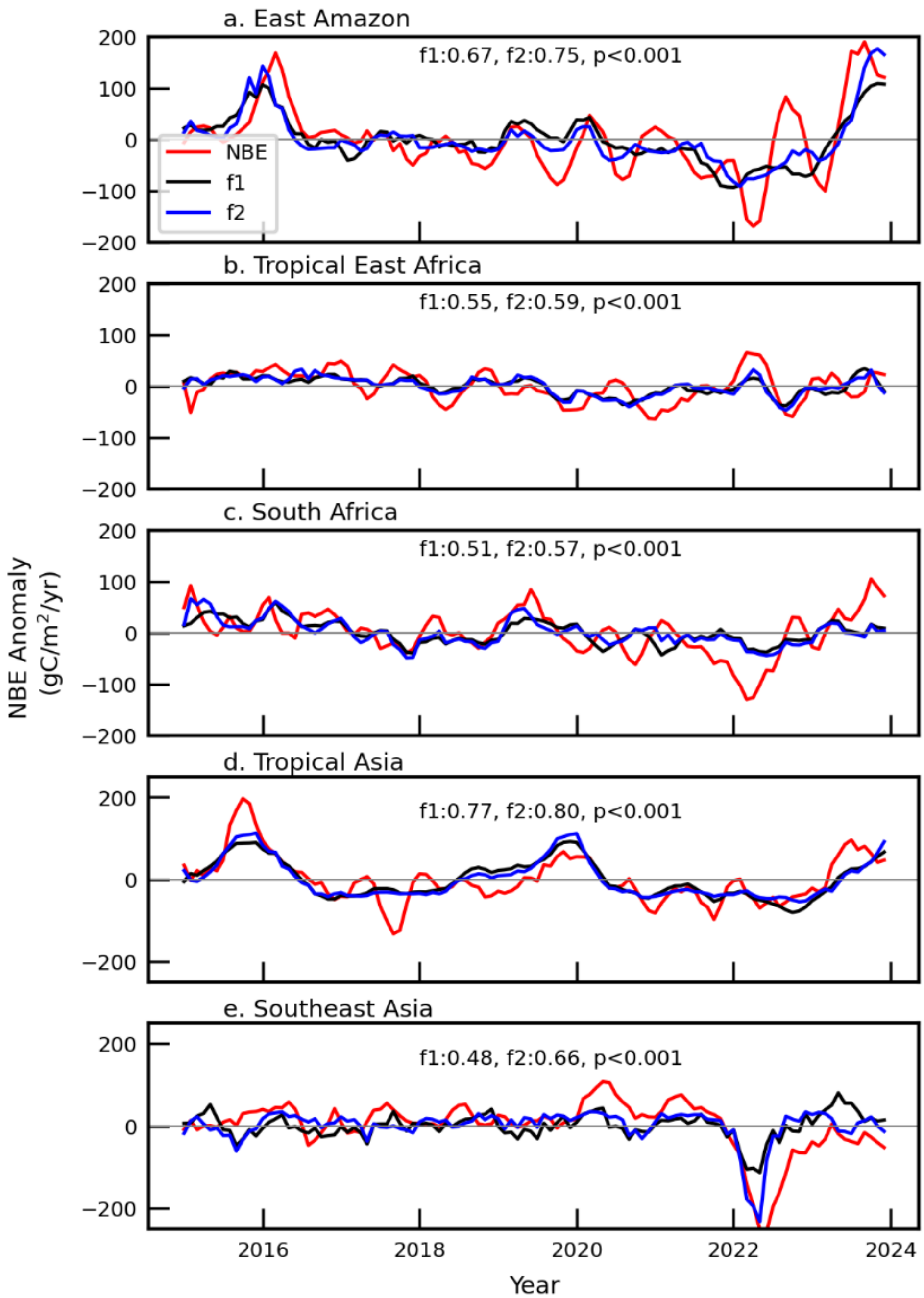

Figure A2 As Figure 5, but for NBE anomalies inferred using OCO-2 land nadir, land glint, and ocean glint data, and *in situ*
555 data.

https://doi.org/10.5194/egusphere-2025-1793
Preprint. Discussion started: 6 May 2025

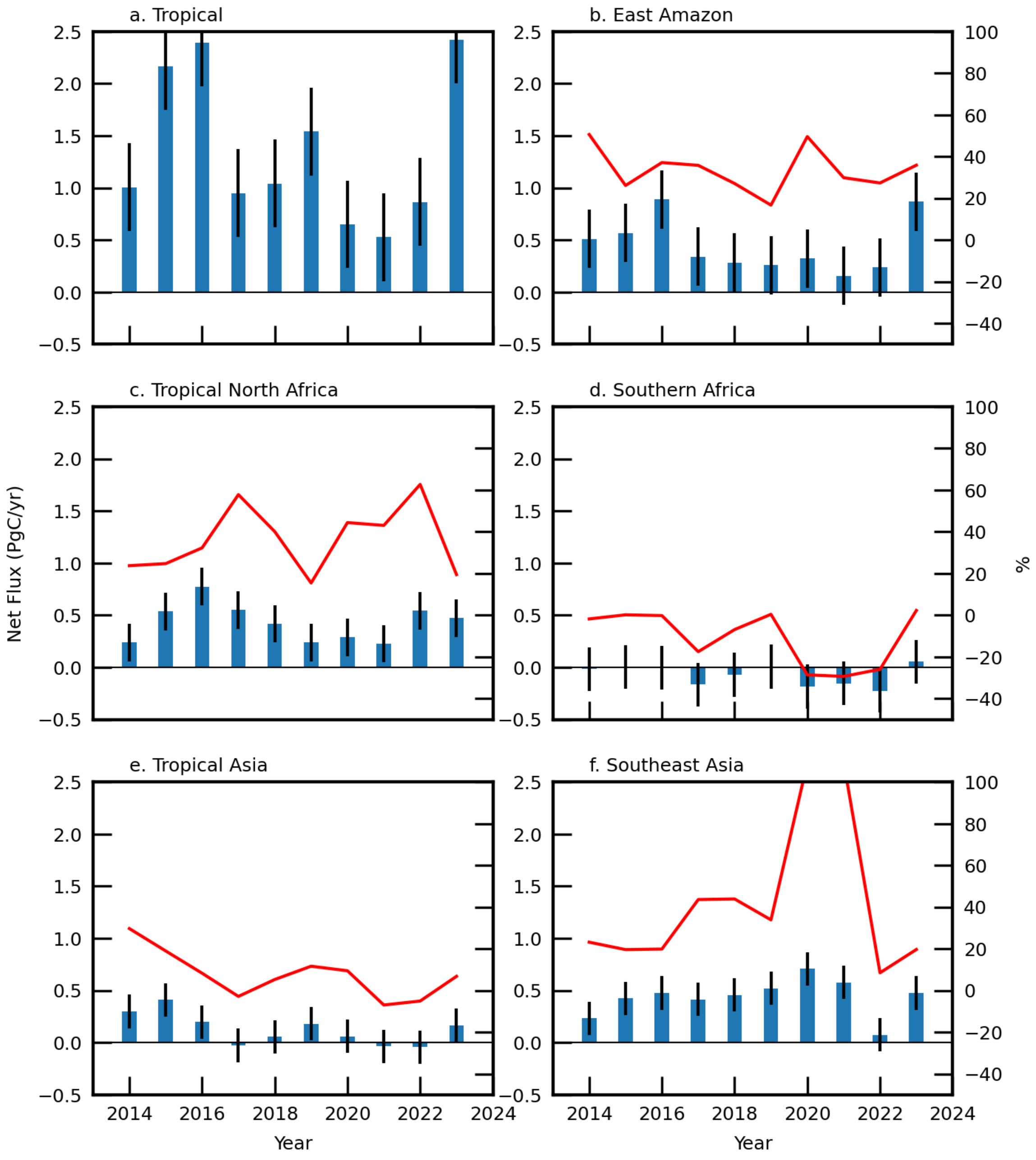

Figure A3 As Figure 2 but for *a posteriori* CO_2 flux estimates across the tropics. Regions are as defined by the rectangles shown in Figure 3a. Percentage values higher than 100% are a consequence of some regional fluxes being negative.

https://doi.org/10.5194/egusphere-2025-1793
Preprint. Discussion started: 6 May 2025

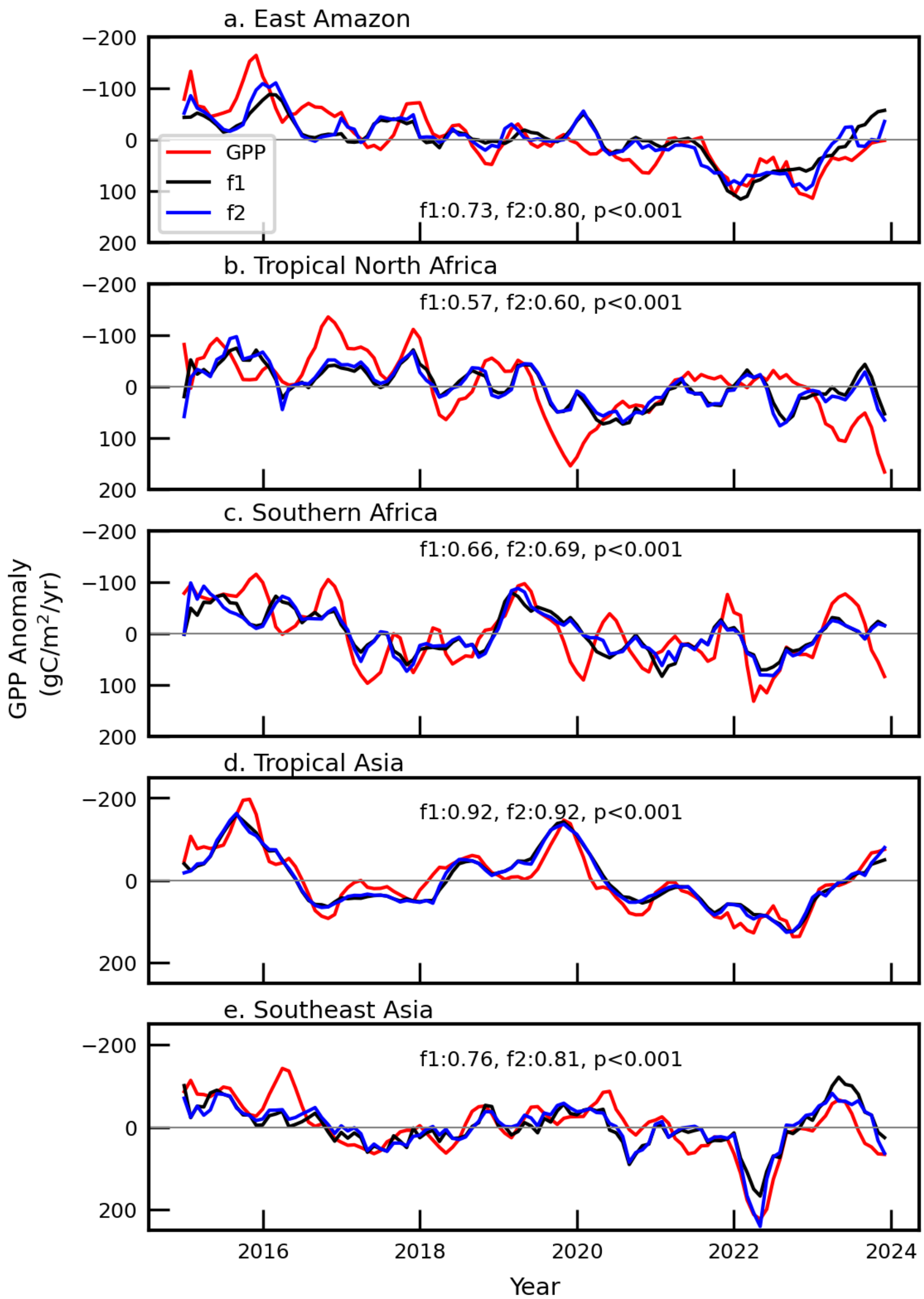

560 **Figure A4**: As Figure 5 but fitting to GOSIF GPP anomalies.

https://doi.org/10.5194/egusphere-2025-1793
Preprint. Discussion started: 6 May 2025

	E. Amazon	NAf	SAf	Tr.Asia	SE.Asia
Rain	-0.05	-0.21	0.18	0.11	-0.42
Surface temperature	0.40	0.09	0.17	0.06	-0.03
Soil moisture	-0.29	-0.51	-0.44	-0.84	-0.11

Table A1 Normalized linear fitting coefficients for the independent variables of the MERRA2 rain, surface temperature, and soil moisture used to fit the NBE anomalies (Figure 5) for the regions defined in Figure 3a. The largest coefficient for each region is highlighted.

https://doi.org/10.5194/egusphere-2025-1793
Preprint. Discussion started: 6 May 2025

Region	Rain	Temp	Soil Moisture	VPD	GOSIF GPP
E.Amazon	<0.01	0.34	0.31	0.01	0.02
NAf	<0.01	0.06	0.51	0.24	0.03
SAf	<0.01	0.06	0.13	0.05	0.66
Tr. Asia	<0.01	0.01	0.32	0.01	0.44
SE.Asia	<0.01	0.02	0.07	0.15	0.62

Table A2 Permutation importance for using variables of the MERRA2 rain, surface temperature, and soil moisture, VPD, and GOSIF GPP to fit the NBE anomalies (Figure 5) for the regions defined in Figure 3a. The largest contributor for each region is highlighted.